X-ray diffraction from d spacing gradients along ion-implanted zones

Satish I. Rao and C. R. Houska

Citation: Journal of Applied Physics **69**, 8096 (1991); doi: 10.1063/1.347459
View online: http://dx.doi.org/10.1063/1.347459
View Table of Contents: http://scitation.aip.org/content/aip/journal/jap/69/12?ver=pdfcov
Published by the AIP Publishing

X-ray diffraction from *d* spacing gradients along ion-implanted zones

Satish I. Rao and C. R. Houska
Department of Materials Engineering, Virginia Polytechnic Institute and State University, Blacksburg, Virginia 24061

(Received 15 December 1989; accepted for publication 15 February 1991)

Three kinematic diffraction models are described for interpreting diffraction profiles from ion-implanted samples. Each deals with relatively large *d* spacing gradients. The first treats the full zone as coherent which requires a direct summation of the Fourier series. The Bragg intensity band from the full zone is applied to implanted zones that are subjected to elastic constraints without incoherent interfaces. For high-fluence samples, and foreign interstitials, a static attenuation term becomes important and is included in all models. This term was not included in previous publications by the authors. The last two models deal with finite subgrain elements that may be connected in a continuous way with interfaces. With a linear element model, slope discontinuities give a sawtooth appearance of the *d* spacing curve. These discontinuities are eliminated by employing a sinusoidal variation in *d* spacing in a third model. The additional smoothing does not provide significant changes in the fine structure of the measured intensity. The parameters that determine line shape are: ΔM, the total change in the attenuation factor M within a subgrain, and $s = N_3 l(\Delta d/\langle d \rangle)$ which contains three additional independent parameters. These are the subgrain size, the order of the Bragg peak l, and the fractional changes in *d* spacing. The static lattice displacements can be large enough to introduce an asymmetry of the diffraction profiles from individual elements. This occurs when ΔM is greater than 0.15. Although this factor has been introduced only into the linear element model, a similar asymmetry should be observed with a sinusoidal variation in *d* spacing.

I. INTRODUCTION

Ion implantation of foreign atoms into a metal lattice results in a near-surface chemical concentration gradient and residual lattice damage. The strain gradient associated with this process is confined to a region generally less than 0.5 μm. X-ray line-shape analysis has been used to extract composition versus depth curves in the case of diffused films,[1] where the strain gradient extends over a few micrometers. In such an analysis, the diffusion zone can be divided into a large number of subgrains, assuming that the *d* spacing (or composition) is essentially a constant within each subgrain. The intensities from all the subgrains, weighted by an average absorption term for each subgrain, is summed to obtain the total intensity profile from the diffusion zone.[2,3] In an ion-implanted zone, the strain can be highly localized giving large apparent strain gradients. Also, the static atomic displacements around certain implant and knock-on defects can produce significant attenuation of the scattered intensity.[4] This is likely to occur when a few percent of interstitial atoms are implanted and/or the lattice damage consists of vacancy and interstitial loops.[4,5]

We treat the diffraction profiles in two ways. For the first, the entire *d* spacing profile is taken to be continuous without sub-boundaries. A second approach treats either a linear or a sinusoidal variation in the *d* spacing within finite subgrains. The effect of static atomic displacements introduces a term that causes a profile to become asymmetric and attenuated. These new developments are used to fit experimental Bragg x-ray intensity bands from ion-implanted samples with a self-consistent near-surface *d* spacing profile.[6]

Our final profile for subgrains, using the linear element model with the attenuation term, is a Fourier series with simplified coefficients. It is shown that a sinusoidal variation in *d* spacing can be related to the Fourier representation of a finite linear element. In this case, the final form is a series of Bessel functions. Under realistic conditions, this intensity expression can be used interchangeably with an exact calculation of the finite linear element model.[7] This implies that discontinuities introduced by straight-line segments, used to approximate continuous *d* spacing curves, do not introduce significant spurious detail into the calculated intensity profiles. Kinematic theory may be used throughout these developments because of the relatively large distortions normally encountered in ion-implantation problems.

II. INTENSITY DISTRIBUTION FROM ELASTIC MODEL

Figure 1 shows a representative sketch of the *d* spacing profile along a multiply ion-implanted zone, and the division of such a zone into connecting linear regions. The assumption of a linear gradient within each subgrain introduces sharp corners in the *d* spacing profile especially when the *d* spacing gradient changes sign in the sawtooth regions. A sinusoidal representation of the *d* spacing gradient within each subgrain eliminates the sawtooth discontinuities. The importance of these discontinuities on the x-ray intensity profile is examined in later sections, by comparing the results from these two models. Our first consideration is an examination of a coherent zone without subgrains. It

 0021-8979/91/128096-08$03.00

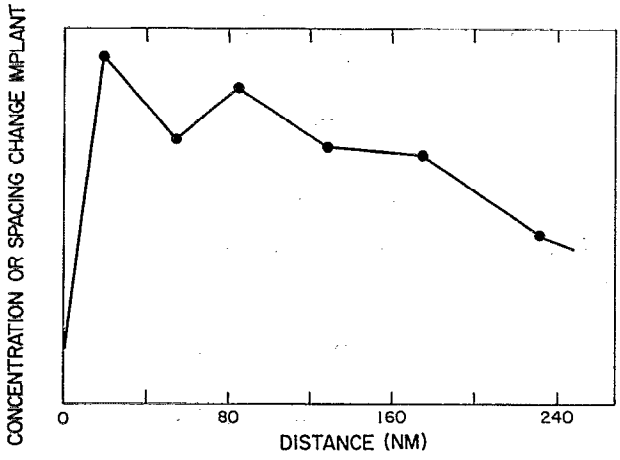

FIG. 1. Linear representation of d spacing or composition profile within subgrains along a multiply implanted zone.

is based upon an elastic calculation making use of the method of strain suppression, which has been discussed elsewhere.[8] The displacement Z_m is obtained by summing to obtain the accumulated strain along the 3 direction at each m position

$$Z_m=\sum_{t=0}^{m}\cdots\epsilon'_{33}(ta_3)=\beta^{el}\sum_{t=0}^{m}\epsilon'_{f33}(ta_3). \tag{1a}$$

This may be written in terms of the fractional change in volume/unit change in concentration and the concentration at each m:

$$Z_m=\beta^{el}\left(\frac{1}{3V}\frac{\partial V}{\partial C}\right)\sum_{t=0}^{m}C(ta_3). \tag{1b}$$

This displacement component, Z_m is magnified by the factor $\beta^{el}=(C_{11}+2C_{12})/(C_{11}+C_{an}\Omega_{hkl})$, due to the formation of residual stresses along the implanted zone.

If the implanted zone is completely constrained by the underlying substrate, then the displacement components along the a_1 and a_2 directions (directions parallel to the free surface), X_m and Y_m, are zero at each position ta_3. Also, the strains normal to the free surface ϵ'_{33} are only a function of ta_3. By introducing these simplications into basic diffraction equations, and summing over each layer, one obtains the following equation for the intensity profile around an (hkl) reflection:

$$I=K'F^2\frac{\sin^2\pi N_1h'_1}{(\pi N_1h'_1)^2}\frac{\sin^2\pi N_2h'_2}{(\pi N_2h'_2)^2}\times\sum_{m_3}\sum_{m'_3}e^{-M(m_3)}e^{-M(m'_3)}$$

$$\times e^{2\pi il(Z_{m_3}-Z'_{m_3})}e^{2\pi i(m_3-m'_3)h_3}, \tag{2}$$

where K' is constant over one intensity band, F is the structure factor for the normal unit cell, N_1a_1 and N_2a_2 are the dimensions of the crystal along the a_1 and a_2 directions parallel to the free surface, and $h'_1=(h_1-h)$, $h'_2=(h_2-k)$, h_3 are variables in reciprocal space expressed in units of the reciprocal axes b_1, b_2, b_3. The exponentials containing $M(m_3)$ and $M(m'_3)$ are static attenuation factors. If N_1a_1 and N_2a_2 are taken to be large, the intensity in reciprocal space is spread only along the h_3 direction, and is a product of δ functions with respect to the h'_1 and h'_2 dependence. The variation of the intensity along the h_3 direction that is normal to the free surface, is obtained by numerically summing Eq. (2). The displacement Z_{m_3} is obtained by summing Eq. (1b) along this direction.

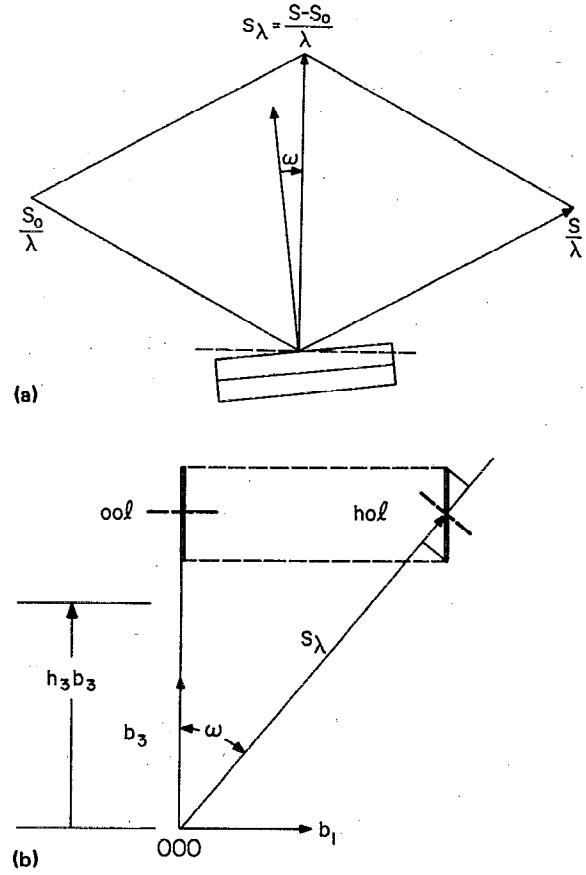

FIG. 2(a). Definition of incident S_0 and signal S direction vectors, tilt angle ω, and diffraction vector S_λ. (b). Schematic drawing of two intensity bands in reciprocal space for a completely elastic zone. Also shown are diffraction vector S_λ at tilt angle ω rocking distance as heavy dashed lines, and the distance h_3b_3. Reciprocal lattice vectors b_1 and b_2 are coplanar and perpendicular to b_3.

The intensity distribution is along the h_3 or the radial direction, when $h=k=0$. For all others, the intensity band remains directed along the h_3 direction in reciprocal space. Under these conditions, radial scans will see a projection of the intensity band. At an angle ω, where ω is the angle of inclination of the (hkl) point with respect to $(00l)$ the projection becomes

$$\cos\omega=l/\sqrt{h^2+k^2+l^2}. \tag{3}$$

When this holds, the spread of the intensity around an (hkl) point along the h_3 direction is identical to the distribution around the corresponding $(00l)$ point (see Fig. 2). A detailed study of the intensity distribution around several (hkl) points in reciprocal space is required to determine ϵ'_{33} and assess whether the strains along the 1′, 2′ directions are zero.

If particle size broadening is negligible, one can show that the broadening Δh_3^B for a linear change in strain is

proportional to ϵl.[2] This remains true if linear elements are superimposed to describe more complex strain distributions. In this case, one treats ϵ as representing the overall distribution of strain characterizing the long range d spacing profile. Under the present conditions, one can interrelate all (hkl) distributions to the corresponding $(00l)$ distribution. This is given by

$$(\Delta S_\lambda/S_\lambda)_{hkl}=(\Delta h_3^B/l)_{00l}\cos^2\omega \tag{4}$$

$$=|\epsilon|\cos^2\omega. \tag{5}$$

Since the radial distance is $|S_\lambda|=2\sin\theta/\lambda$ and the spread of intensity is small, one can show by differentiation that

$$\Delta 2\theta(\text{rad})=2(\epsilon\cos^2\omega)\tan\theta. \tag{6}$$

This gives the typical $\tan\theta$ relation between a shift in d spacing and the related angular change. The additional $\cos^2\omega$ allows for projections along the tilt angle ω. If this dependence is obeyed, then the purely elastic model is verified and particle size broadening is negligible. These data are examined in a later paper.

The free expansion model can be restricted to spacing changes that vary only with m. For each layer of fixed composition, there are rows of cells having the periodicity a_1 and a_2. However, because adjacent layers may have different compositions and periodicities a_1, a_2, the overall effect will be broadening along $[hk0]$ directions in reciprocal space. Tilting the sample from $\omega=0°$ to 90° will not give a systematic sharpening of radial diffraction scans according to Eq. (6). This problem is further complicated if the elastic relaxations result from dislocation arrays. Additional line broadening could be observed due to incomplete cancellation of the dislocation fields extending from each interface. However, the most characteristic feature is the absence of the elastic magnification factor, β^{el}. In other words, the displacements along the sample normal will be determined by the free expansion rather than by the combined effects of free and elastic expansions.

III. CALCULATIONS

A. Subgrain with linear change in *d* spacing

Consider a subgrain, with a thickness $N_3\langle d\rangle$ along the z axis. N_3 is the number of diffracting layers within each subgrain, and $\langle d\rangle$ is the average d spacing of the $(00l)$ reflection planes, which changes linearly from $\langle d\rangle-[(N_3-1)/2]\Delta$ at $R=0$, to $\langle d\rangle+[(N_3-1)/2]\Delta$ at $R=N_3\langle d\rangle$. The d spacing between the m and $m-1$ layers is equal to $\langle d\rangle-[(N_3-1)/2]\Delta+(m-1)\Delta$, with Δ representing the spacing increment. The amplitude of scattering from such a subgrain, as a function of the reciprocal space variable, $h_3=2\langle d\rangle\sin\theta/\lambda$ measured parallel to z axis, is given by

$$A(h_3)=K'\sum_{m=0}^{N_3}F_m\exp(2\pi i Z_m h_3)\exp(2\pi i m h_3), \tag{7}$$

where $Z_m=(\mathrm{R(m)}-\mathrm{m}\langle\mathrm{d}\rangle)/\langle\mathrm{d}\rangle$, R(m) is the position of the mth reflecting layer from the origin ($R=0$) along the z axis, K' is a constant, θ is the Bragg angle, λ the x-ray wavelength, and F_m, the scattering factor of the mth layer. The intensity profile is equal to[9,10]

$$I(h_3)=K\sum_{m=0}^{N_3}\sum_{m'=0}^{N_3}F_mF_{m'}^*\exp[2\pi i(Z_m-Z_{m'})h_3]$$

$$\times\exp[2\pi i(m-m')h_3], \tag{8}$$

where K is a constant over one peak. The double summation can be reduced to a single summation,

$$I(h_3)=KN_3F_0^2\sum_{n=-N_3}^{N_3}G_n\exp(2\pi i n h_3), \tag{9}$$

where G_n is the normalized Fourier coefficient, given by

$$G_n=\frac{1}{N_3}\sum_{m=n}^{N_3}e^{-M(m)}e^{-M(m-n)}$$

$$\times\exp[2\pi i l(Z_m-Z_{m-n})], \tag{10}$$

for n positive with

$$G_{-n}=G_{+n}^*.$$

F_0 is the unattenuated scattering factor of each layer of thickness equal to one cell height, $e^{-M(m)}$ and $e^{-M(m-n)}$ are the static displacement attenuation factors for the m(th) and $(m-n)$th layers respectively, and l is the order of the reflection. In Eq. (3) the sum is taken over all possible pairs of layers, separated by a distance $n\langle d\rangle$. Equation (10) can be expressed as an integral,

$$I(h_3)=KN_3^2F_0^2\int_{-1}^{+1}G_n\exp(2\pi i h_3^0 u)du, \tag{11}$$

where $h_3^0=N_3h_3$ and $u=n/N_3$ are dimensionless. For a linear change in d spacing the position of the mth layer from the origin is determined by evaluating an arithmetic sum which gives

$$R(m)=m\langle d\rangle-[m(N_3-1)/2]\Delta+\{[m(m-1)]/2\}\Delta \tag{12}$$

and

$$\exp[2\pi i l(Z_m-Z_{m-n})]$$

$$=\exp\{-2\pi i l n[(N_3-1)/2]\Delta\}$$

$$\times\exp\{2\pi i l[(2mn-n^2-n)/2](\Delta/\langle d\rangle)\}. \tag{13}$$

The d spacing gradient results from a concentration gradient of implants and lattice defects. If one type of defect predominates, the relative change in d spacing between neighboring layers, $\Delta/\langle d\rangle$, is linearly proportional to the change in concentration of defects from layer to layer, Δc, and for a cubic crystal is given by

$$\frac{\Delta}{\langle d\rangle}=\frac{\beta\Delta c}{3}\left(\frac{1}{V}\frac{\partial V}{\partial C}\right), \tag{14a}$$

where β is a proportionality constant defined for the extreme conditions of complete plastic or complete elastic deformation. This is produced by constraining forces from undisturbed underlying material and volume changes in the implanted zone.[8] For complete plastic deformation,

$$\beta^p=1, \tag{14b}$$

and if the element remains completely elastic, the effect is enhanced by the factor

$$\beta^{el}=(C_{11}+2C_{12})/(C_{11}+C_{an}\Omega_{hkl}), \tag{14c}$$

since this is greater than unity. $C_{an} = C_{44} - \frac{1}{2}(C_{11} - C_{12})$, C_1, C_{12}, and C_{44} are the cubic elastic constants. $\Omega_{hkl} = 4(\alpha_3^2\beta_3^2 + \alpha_3^2\gamma_3^2 + \beta_3^2\gamma_3^2)$, and α_3, β_3, and γ_3 are the direction cosines of the normal to the free surface (z axis) and the edges of the cubic unit cell. β is further discussed in another paper.[8] $(1/v)(\partial v/\partial c)$ is the fractional change in volume due to the addition of a unit concentration of point defects. If more than one type of point defect predominates, then

$$\frac{\Delta}{\langle d\rangle}=\frac{\beta}{3}\sum_i \Delta c_i\left(\frac{1}{v}\frac{\partial v}{\partial c}\right)_i, \tag{15}$$

where the summation over i extends over all defects. The scattering factor of the mth layer is attenuated by $e^{-M(m)}$, where $M(m)$ is linearly proportional to the concentration of defects.[4,5] For one kind of defect,

$$M(m)=M_0+m\alpha\Delta c, \tag{16}$$

where α is a proportionality constant between attenuation factor M and the concentration of point defects, c. M_0 is the attenuation factor at the origin of the subgrain. α depends upon $(\sin\theta/\lambda)^2$ and the type of point defects.[4,5] From Eq. (16), the value of the product $e^{-M(m)}e^{-M(m-n)}$ becomes

$$e^{-M(m)}e^{-M(m-n)}$$

$$=\exp(-2M_0)\exp(n\alpha\Delta c)\exp(-2m\alpha\Delta c). \tag{17}$$

Substituting Eqs. (17) and (13) into Eq. (10), with $m=m'+n$,

$$G_{+n}=\frac{1}{N_3}\exp(-n\alpha\Delta c)\exp(-2M_0)$$

$$\times\exp\left(-i\pi ln(N_3-n)\frac{\Delta}{\langle d\rangle}\right)$$

$$\times\sum_{m'=0}^{N_3-n}\exp\left[2\pi i\ell m' n\left(\frac{\Delta}{\langle d\rangle}+\frac{i\alpha\Delta c}{\pi ln}\right)\right]. \tag{18}$$

The geometrical summation in Eq. (18) gives

$$G_{+n}=\frac{e^{-2\langle M\rangle}}{N_3}\frac{\sin[\pi u(1-u)(s+i\Delta M/\pi u)]}{\sin(\pi u/N_3(s+i\Delta M/\pi u)}$$

$$\simeq e^{-2\langle M\rangle}\frac{\sin[\pi u(1-u)(s+i\Delta M/\pi u)]}{\pi u(s+i\Delta M/\pi u)},$$

$$G_{-n}=G^*_{+n}, \tag{19}$$

with $s=N_3 l\Delta d/\langle d\rangle$. $\Delta M=\alpha N_3\Delta c$, and $\Delta d=N_3\Delta$ represent the total change in M and d spacing from one end of the subgrain to the other. $\langle M\rangle$ is the attenuation factor, at $m=N_3/2$. Equation (19) shows that the Fourier coefficient is complex, which introduces an asymmetry about the point $h_3=l$. For substitutional solid solutions, α and M are usually negligible and the attenuation factor and imaginary term may be dropped giving Eq. (19) of Ref. 2. The asymmetry is caused by the variation in attenuation factor within each subgrain. If the variation in attenuation factor is small or $\Delta M\to 0$, an exact result can be obtained for the intensity profile[7]

$$I(h_3)_{\alpha,\Delta M=0}=\frac{KN_3^2}{2s}\langle F\rangle^2\left(\left\{C\left[\left(\frac{2}{s}\right)^{1/2}\left(\frac{s}{2}-h_3^0\right)\right]\right.\right.$$

$$\left.+C\left[\left(\frac{2}{s}\right)^{1/2}\left(\frac{s}{2}+h_3^0\right)\right]\right\}^2$$

$$+\left\{S\left[\left(\frac{2}{s}\right)^{1/2}\left(\frac{s}{2}-h_3^0\right)\right]\right.$$

$$\left.\left.+S\left[\left(\frac{2}{s}\right)^{1/2}\left(\frac{s}{2}+h_3^0\right)\right]\right\}^2\right), \tag{20}$$

where C and S, in this expression, are the cosine and sine Fresnel integrals,[11] and $\langle F\rangle = F_0 e^{-\langle M\rangle}$. The behavior of this function, symmetric about $h_3=l$, has already been discussed.[7] For $s=0$, Eq. (14) gives only particle size broadening. However with $s>1$, the effect of the strain gradient on the intensity profile becomes important and depends upon the product of $N_3 l(\Delta d/\langle d\rangle)$ rather than any one of these terms by itself. Typical values of s range from 0–4 for those ion-implanted zones we have encountered.[6]

Equation (19) with α and $\Delta M\neq 0$ has to be summed or transformed numerically using Eqs. (9) or (10), in order to obtain the intensity profile. Figure 3 shows plots of the intensity profile from a subgrain with $s=4$, $\Delta M=0.0$, and 0.5. As $|\Delta M|$ increases, the intensity profile becomes more and more asymmetric and the maxima of the profile shifts away from $h_3=l$, towards a lower concentration of implant. Static atomic displacements around point defects produce significant effects on the diffraction profile if the product of terms containing α and $N_3\Delta c$ is sufficiently large across a subgrain. This has been found for N implanted into Nb to an average level of 5 at. % using four energies.[10] Equation (19) can be applied when more than one type of point defect is important, by superimposing their fields, i.e.,

$$\Delta M=N_3\sum_i \alpha_i\Delta c_i. \tag{21}$$

The total intensity from the subgrain can be obtained by integrating Eq. (11) with Eq. (19) over each (hkl) profile, i.e.,

$$\int_{-\infty}^{\infty} I(h_3)dh_3=KN_3F_0^2(G_n)_{n=0}$$

$$=KN_3\langle F\rangle^2\frac{e^{\alpha N_3\Delta c}-e^{-\alpha N_3\Delta c}}{2\alpha N_3\Delta c},$$

or $KF_0^2\int_{m=0}^{N_3} e^{-2M(m)}dm$ which requires

$$\langle e^{-2M}\rangle = e^{-2\langle M\rangle}\frac{e^{\alpha N_3\Delta c}-e^{-\alpha N_3\Delta c}}{2\alpha N_3\Delta c}. \tag{22}$$

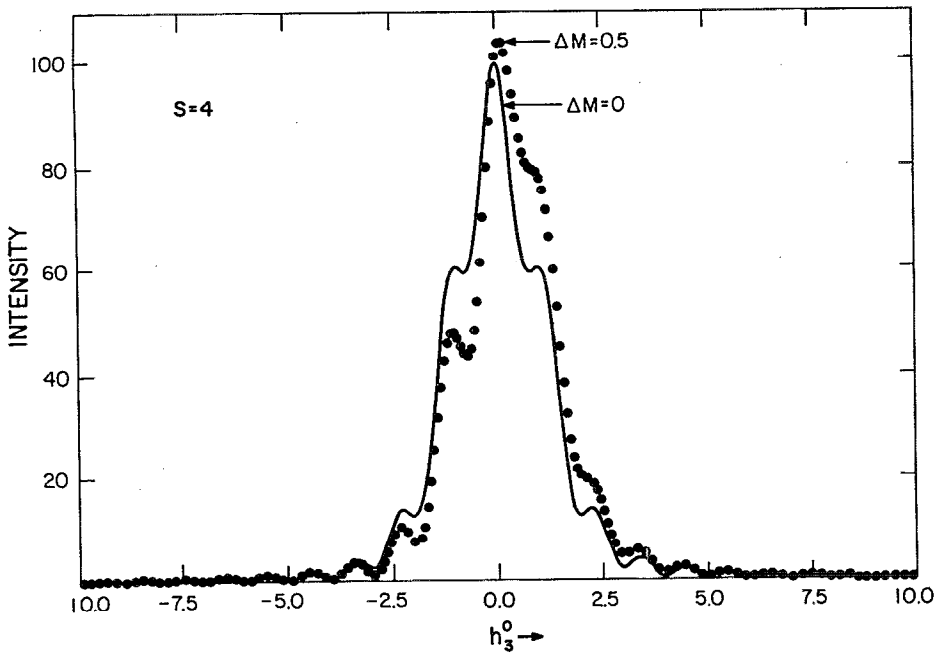

FIG. 3. Symmetrical ($\Delta M = 0$) and asymmetrical ($\Delta M = 0.5$) intensity profiles for a finite linear subgrain with $S = 4$ illustrating the importance of static displacements.

This result becomes useful in determining $\langle M \rangle$ for an implanted sample.

B. Subgrain with sinusoidal change in *d* spacing

In this section, we develop the intensity profile from a sample having a sinusoidal variation in spacing and compare the results, with one having a linear change in spacing. This leads to useful conclusions even though a constant attenuation factor ($\alpha = 0$) is used for each element. We start by writing the linear d spacing gradient extending from $\langle d \rangle - (\Delta d/2)$ at $R = 0$ to $\langle d \rangle + \Delta d/2$ at $R = N_3\langle d \rangle$ as a Fourier series,

$$d(R) = \langle d \rangle - \frac{4\Delta d}{\pi^2} \sum_{t=0}^{\infty} \frac{\cos(2t+1)(\pi R/L)}{(2t+1)^2}, \qquad (23)$$

where R is the distance from the origin of the subgrain $m\langle d \rangle$, and L is the subgrain thickness $N_3\langle d \rangle$. Consider only the first two terms in the expansion, i.e.,

$$d(R) \cong \langle d \rangle - \frac{4\Delta d}{\pi^2} \cos\frac{\pi R}{L}, \quad 0 \leqslant R \leqslant L. \qquad (24)$$

The d spacing profile of Eq. (24) changes in a sinusoidal fashion from $\langle d \rangle - 4\Delta d/\pi^2$ at $R = 0$ $(m = 0)$ to $\langle d \rangle + 4\Delta d/\pi^2$ at $R = L$ $(m = N_3)$ with a value of $\langle d \rangle$ at the midpoint. Figure 4 illustrates a linear d spacing profile as well as the two-term Fourier series approximation of the profile, obtained from Eq. (25). Several authors have treated the diffraction problem from a periodic d spacing profile, but with an infinite subgrain thickness.[12,13] Such a treatment is not applicable here, since it neglects the effect of subgrain size on x-ray broadening.

The position of the mth layer from the origin can be calculated from Eq. (24) resulting in

$$Z_m = -\frac{4\Delta d}{\pi^2\langle d \rangle} \sum_{t=0}^{m-1} \cos\frac{\pi t\langle d \rangle}{L} \cong -\frac{4N_3\Delta d}{\pi^3\langle d \rangle} \sin\frac{\pi m}{N_3}. \qquad (25)$$

With $e^{-M(m)} = e^{-M(m-n)} = e^{-\langle M \rangle}$, and by substituting Eq. (25) into Eq. (10), one obtains

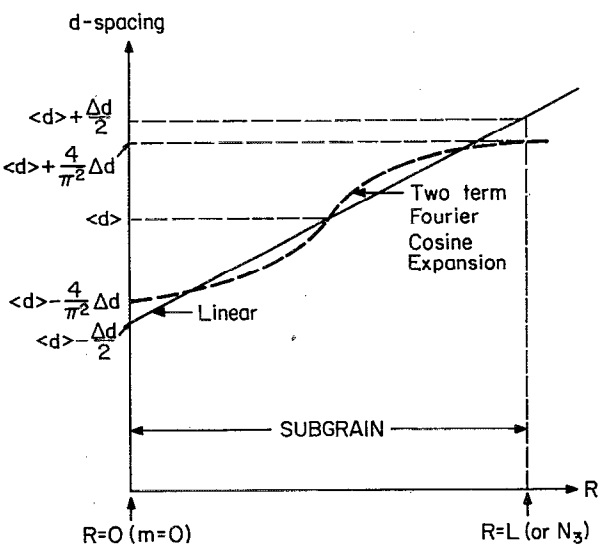

FIG. 4. Two-term cosine expansion of linear model with thickness L (or N_3) showing end-point spacings for both relative to the central value $\langle d \rangle$.

$$G_{+n}=\frac{e^{-2\langle M\rangle}}{N_3}\sum_{m=n}^{N_3}\exp\left(-i\frac{8}{\pi^2}s\sin\frac{\pi}{N_3}m\right)\exp\left(i\frac{8}{\pi^2}s\sin\frac{\pi}{N_3}(m-n).\right) \tag{26}$$

The exponentials in Eq. (26) can be expanded as a Fourier–Bessel series from Eqs. (9.1.42) and (9.1.43) in Ref. 11, giving

$$G_{+n}=\frac{e^{-2\langle M\rangle}}{N_3}\sum_{m=n}^{N_3}\left(J_0(z)-2i\sum_{t=0}^{\infty}J_{2t+1}(z)\sin\frac{(2t+1)\pi m}{N_3}+2\sum_{t'=1}^{\infty}J_{2t'}(z)\cos\frac{2t'\pi m}{N_3}\right)$$
$$\times\left(J_0(z)+2i\sum_{t''=0}^{\infty}J_{2t''+1}(z)\sin\frac{(2t''+1)\pi(m-n)}{N_3}+2\sum_{t'''=1}^{\infty}J_{2t'''}(z)\cos\frac{2t'''\pi(m-n)}{N_3}\right), \tag{27}$$

with $z=(8/\pi^2)s$, and $J_n(z)$ the value of the Bessel function of order n at z. After summing over t this becomes

$$G_{+n}=e^{-2\langle M\rangle}\left[J_0^2(z)\left(1-\frac{n}{N_3}\right)+2\sum_{t=1}^{\infty}J_t^2(z)\left(1-\frac{n}{N_3}\right)\cos\frac{\pi tn}{N_3}\right]+2\sum_{t=1}^{\infty}(-1)^{t+1}\frac{J_t^2(z)}{t\pi}\sin\frac{t\pi n}{N_3}$$
$$-2J_0(z)\sum_{t=1}^{\infty}\frac{J_{2t}(z)}{t\pi}\sin\frac{2t\pi n}{N_3}+\frac{4}{\pi}\sum_{\substack{t=2\\ t>t'}}^{\infty}\sum_{t'=1}^{\infty}J_{2t}(z)J_{2t'}(z)$$
$$\times\left(\frac{t'}{t^2-t'^2}\sin\frac{2t'n}{N_3}-\frac{t}{t^2-t'^2}\sin\frac{2t\pi n}{N_3}\right)+\frac{8}{\pi}\sum_{\substack{t=1\\ t>t'}}^{\infty}\sum_{t'=0}^{\infty}J_{2t+1}(z)J_{2t'+1}(z)$$
$$\times\left(\frac{2t+1}{(2t+1)^2-(2t'+1)^2}\sin\frac{(2t'+1)\pi n}{N_3}-\frac{2t'+1}{(2t+1)^2-(2t'+1)^2}\sin\frac{(2t+1)\pi n}{N_3}\right), \tag{28}$$

$$G_{-n}=G_{+n}.$$

Equation (28) can be Fourier transformed analytically giving the following intensity profile:

$$I(h_3)=KN_3^2\langle F\rangle^2\left\{J_0^2(z)\frac{\sin^2\pi h_3^0}{(\pi h_3^0)^2}+\sum_{n=1}^{\infty}J_0^2(z)\left(\frac{\sin^2\pi h_3^{0,n+}}{(\pi h_3^{0,n+})^2}+\frac{\sin^2\pi h_3^{0,n-}}{(\pi h_3^{0,n-})^2}\right)+2\sum_{n=1}^{\infty}(-1)^{n+1}\frac{J_n^2(z)}{n\pi}\right.$$
$$\times\left(\frac{\sin^2\pi h_3^{0,n+}}{\pi h_3^{0,n+}}-\frac{\sin^2\pi h_3^{0,n-}}{\pi h_3^{0,n-}}\right)-2J_0(z)\sum_{n=1}^{\infty}\frac{J_{2n}(z)}{n\pi}\left(\frac{\sin^2\pi h_3^{0,2n+}}{\pi h_3^{0,2n+}}-\frac{\sin^2\pi h_3^{0,2n-}}{\pi h_3^{0,2n-}}\right)+\frac{4}{\pi}$$
$$\times\sum_{\substack{n=2\\ n>n'}}^{\infty}\sum_{n'=1}^{\infty}J_{2n}(z)J_{2n'}(z)\left[\frac{n'}{n^2-n'^2}\left(\frac{\sin^2\pi h_3^{0,2n'+}}{\pi h_3^{0,2n'+}}-\frac{\sin^2\pi h_3^{0,2n'-}}{\pi h_3^{0,2n'-}}\right)-\frac{n}{n^2-n'^2}\right.$$
$$\left.\times\left(\frac{\sin^2\pi h_3^{0,2n+}}{\pi h_3^{0,2n+}}-\frac{\sin^2\pi h_3^{0,2n-}}{\pi h_3^{0,2n-}}\right)\right]+\frac{8}{\pi}\sum_{\substack{n=1\\ n>n'}}^{\infty}\sum_{n'=0}^{\infty}J_{2n+1}(z)J_{2n'+1}(z)\left[\frac{2n+1}{(2n+1)^2-(2n'+1)^2}\right.$$
$$\left.\left.\times\left(\frac{\sin^2\pi h_3^{0,2n'+1+}}{\pi h_3^{0,2n'+1+}}-\frac{\sin^2\pi h_3^{0,2n'+1-}}{\pi h_3^{0,2n'+1-}}\right)-\frac{2n'+1}{(2n+1)^2-(2n'+1)^2}\left(\frac{\sin^2\pi h_3^{0,2n+1+}}{\pi h_3^{0,2n+1+}}-\frac{\sin^2\pi h_3^{0,2n+1-}}{\pi h_3^{0,2n+1-}}\right)\right]\right\}, \tag{29}$$

where

$$h_3^{0,jn+k^{\pm}}=h_3^0\pm(jn+k)/2;\quad j=1\text{ or }2,\ k=0\text{ or }1,$$
$$\text{and } h_3^0=N_3(h_3-l).$$

The Bessel functions can be generated using the usual recurrence relation

$$J_{n+1}(z)=(2n/z)J_n(z)-J_{n-1}(z), \tag{30}$$

and polynomial approximations given for $J_0(z)$ and $J_1(z)$. $I(h_3)$ is symmetric and $h_3=l$. A criterion for truncation can be determined by considering the integrated intensity of the reflection, i.e.,

$$\int_{-\infty}^{\infty}I(h_3)dh_3$$
$$=KN_3F_0^2G_0=KN_3\langle F\rangle^2\left(J_0^2(z)+2\sum_{n=1}^{\infty}J_n^2(z)\right). \tag{31}$$

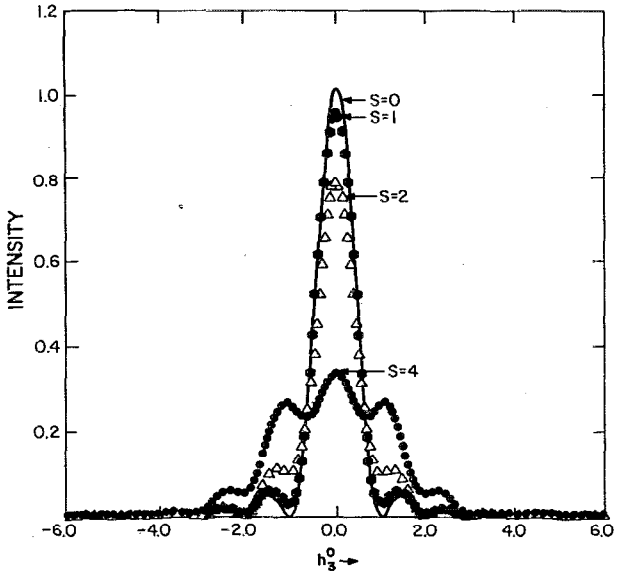

FIG. 5. Intensity profiles for two-term cosine expansion illustrating importance of s.

The integrated intensity of the reflection is identically equal to $KN_3\langle F\rangle^2$ if the summation over n in Eq. (31) is taken to ∞. However, a reasonable upper limit for the number of terms required in Eq. (29) can be attained by satisfying

$$J_0^2(z) + 2\sum_{n=1}^{m} J_n^2(z) \geqslant 0.99. \tag{32}$$

The summations over n in Eq. (29) can be truncated beyond $n \simeq z+2$, for values of z between 0–10, since $J_n(z)$ for $n > z+2$ is essentially zero.[11]

Figure 5 shows plots of Eq. (29) as a function of h_3^0, for $s=0$, 1, 2, 4, which is a typical range for an ion-implanted sample. As s increases from zero, the intensity profile deviates from pure particle size broadening, and strain gradient broadening becomes increasingly significant. This behavior is similar to the one obtained from the linear model, i.e., Eq. (13).

Figure 6 shows the similarity between x-ray intensity profiles from the linear strain gradient [Eq. (13)] and the two-term Fourier expansion [Eq. (29)]. For $s=3$, the profile from the two-term Fourier expansion is in reasonable agreement with the linear gradient model. The mean differences in the two profiles at $s=3$ is equal to $\simeq 2\%$. For $s>4$, the Fourier series expansion clearly has to be taken to more than two terms for the linear gradient model and the series expansion to be in agreement. One can conclude that the major features from composite d spacing profiles may be obtained from the linear gradient model. This also allows one to incorporate the variation in attenuation factor and thereby account for asymmetric profiles.

IV. SUMMARY

We have examined three models describing diffraction profiles from ion-implanted samples containing relatively

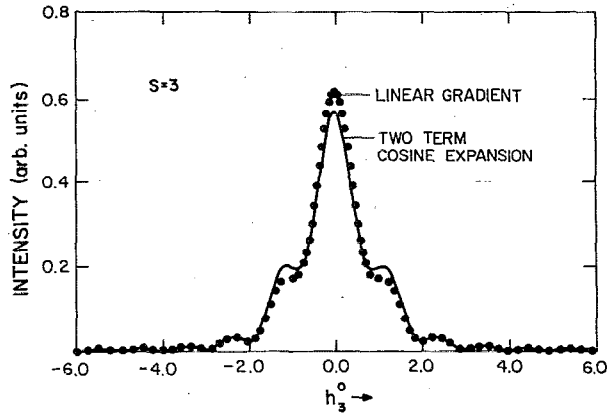

FIG. 6. Comparison of profiles from two models at $s=3$.

large gradients. The first deals with a direct summation of the Fourier series describing the intensity band from the full zone subjected to elastic constraints imposed by the sample. The elastic constraint produces an expanded distribution of d spacing which expands the intensity band. For high-fluence samples and foreign interstitials, the static attenuation becomes important. The intensity distributions are oriented along a direction normal to the free surface.

The last two models deal with subgrain elements that may be connected in a continuous way to approximate more complicated profiles obtained from ion-implanted samples containing incoherent interfaces. With a linear element model, slope discontinuities give a sawtooth appearance of the d spacing curve. These discontinuities may be eliminated with a sinusoidal variation in d spacing. A disadvantage with the latter is the diffraction equation from a finite element is more complicated, and the additional smoothing does not provide significant changes in the fine structure of the simulated intensity.

The important parameters that influence line shape are ΔM (the total change in the attenuation factor M across a subgrain) and $s = N_3(\Delta d/d)$, which contains three additional independent parameters. It was found that the overall diffraction profiles from the linear element model agree within 2% if $s \leqslant 3$ and within 10% if $s \leqslant 4$. For $s>4$, the sinusoidal calculation requires extra terms and a comparison cannot be made at this time.

For implants tending to form interstitial solid solutions and/or cases where there is sufficient lattice damage, the static lattice displacements can be large enough to introduce an asymmetry of the diffraction profiles from individual elements. This occurs when ΔM is greater than about 0.15. Although, this factor has only been introduced into the linear element model as a modified Fourier coefficient, a similar asymmetry is expected with a sinusoidal variation in d spacing. An application of these findings will be given in a forthcoming experimental paper.[6]

ACKNOWLEDGMENTS

This research was sponsored by Office of Naval Research Grant No. N00014-83-K-0750, P00004.

[1] C. R. Houska, in *Treatise on Materials Science and Technology, Experimental Methods,* edited by H. Herman (Academic, New York, 1980), Vol. 19A, p. 63.
[2] C. R. Houska, J. Appl. Phys. **41**, 69 (1970).
[3] C. R. Houska, J. Appl. Phys. **49**, 2991 (1978).
[4] M. A. Krivoglaz, *Theory of X-ray and Thermal Neutron Scattering in Real Crystals* (Plenum, New York, 1969).
[5] P. H. Dederichs, J. Phys. F **3**, 471 (1973).
[6] S. I. Rao, B. He, C. R. Houska, and K. Grabowski, companion paper.
[7] S. I. Rao and C. R. Houska, Acta Cryst. A **41**, 513 (1985).
[8] S. I. Rao and C. R. Houska, J. Mater. Sci. **25**, 2822 (1990).
[9] B. E. Warren, *X-ray Diffraction* (Addison-Wesley, New York, 1969).
[10] A. Guinier, *X-ray Diffraction in Crystals, Imperfect Crystals and Amorphous Bodies* (W. H. Freeman, San Francisco, 1963).
[11] M. Abramowitz and I. Stegun, "Handbook of Mathematical Functions," Washington, DC, U.S. Government Printing Office.
[12] A. Kochendorfer, Z. Kristallogr. **101**, 149 (1939).
[13] A. J. C. Wilson, *X-ray Optics* (Wiley, New York, 1962).